J. Quant. Spectrosc. Radiat. Transfer Vol. 46, No. 4, pp. 293–297, 1991
Printed in Great Britain.

0022-4073/91 $3.00 + 0.00

VARIABLE TEMPERATURE PRESSURE BROADENING OF HNO_3 IN THE MILLIMETER WAVE SPECTRAL REGION

THOMAS M. GOYETTE,†,‡ WEI GUO,† FRANK C. DELUCIA,† and PAUL HELMINGER§

†Department of Physics, Duke University, Durham NC 27706 and §Department of Physics, University of South Alabama, Mobile, AL 36688, U.S.A.

(Received 12 February 1991)

Abstract—The O_2 and N_2 pressure-broadening parameters of the $18_{0,18}$–$17_{0,17}$, $22_{7,15}$–$21_{7,14}$, and $29_{0,29}$–$28_{0,28}$ transitions in the ground vibrational state of HNO_3 have been measured in the temperature range between 100 and 380 K. Above 190 K the measurements were made in an equilibrium cell. Below 190 K, a cell with collisional cooling to circumvent the temperature limits imposed by the vapor pressure of the sample gas was used. The data were fit to the usual exponential temperature dependence with resultant n values ranging from 0.67(5) to 0.84(10) for O_2 and from 0.62(3) to 0.74(9) for N_2.

INTRODUCTION

HNO_3 plays an important role in the chemistry of the upper atmosphere and therefore its line frequencies have been extensively studied in the microwave and infrared (i.r.).[1] However, there have been relatively few data on the pressure-broadening parameters, particularly at temperatures other than room temperature.[2–5] This is understandable since HNO_3 decomposes rapidly at temperatures above 400 K and since low-temperature measurements are ordinarily limited by its vapor pressure, which becomes very small even at 200 K. To circumvent the limitations imposed by the vapor pressure of the sample gas, we have developed a method, known as collisional cooling, for the study of gas-phase samples at temperatures far below the point at which the samples freeze.[6–8] We have also developed a variable temperature equilibrium cell for use at temperatures which permit a large vapor pressure of the sample gas to be sustained in the cell. We have recently used these techniques to study the O_2, N_2, and He pressure-broadening of H_2O in the 80–600 K temperature range.[9]

In this paper we present the O_2 and N_2 pressure-broadening coefficients for the $18_{0,18}$–$17_{0,17}$, $22_{7,15}$–$21_{7,14}$, and $29_{0,29}$–$28_{0,28}$ transitions in the ground vibrational state of HNO_3 in the temperature range from 100 to 380 K. The results are compared with the previous air-broadening study of May and Webster[5] and with the previous Anderson theory calculations of Tejwani and Yeung.[10] We find that a simple power-law equation is sufficient to describe the temperature variation of the pressure-broadening parameters even to the lowest temperatures reported here, in contrast to a drop off below the power law at low temperatures which was seen in our previous study of H_2O. These results, along with our previous room-temperature study of HNO_3 over a wide range of quantum states,[2] should be applicable to the calculation of pressure-broadening parameters in the i.r.

EXPERIMENTAL DETAILS

We have discussed the experimental details of our variable temperature pressure-broadening techniques in a recent paper.[9] Briefly, for temperatures above 190 K, which is a rough lower limit on the usable vapor pressure of HNO_3, a conventional equilibrium cell was used. The cell consists of a quartz tube in an oven with a temperature variable between 80 and 600 K. The oven extends beyond the cell to ensure that the windows are maintained at the same temperature as the cell.

The collisional cooling cell, used at temperatures below 190 K, is shown in Fig. 1.

‡To whom all correspondence should be addressed: Department of Physics, The Ohio State University, 174 West 18th Avenue, Columbus, OH 43210-1106, U.S.A.

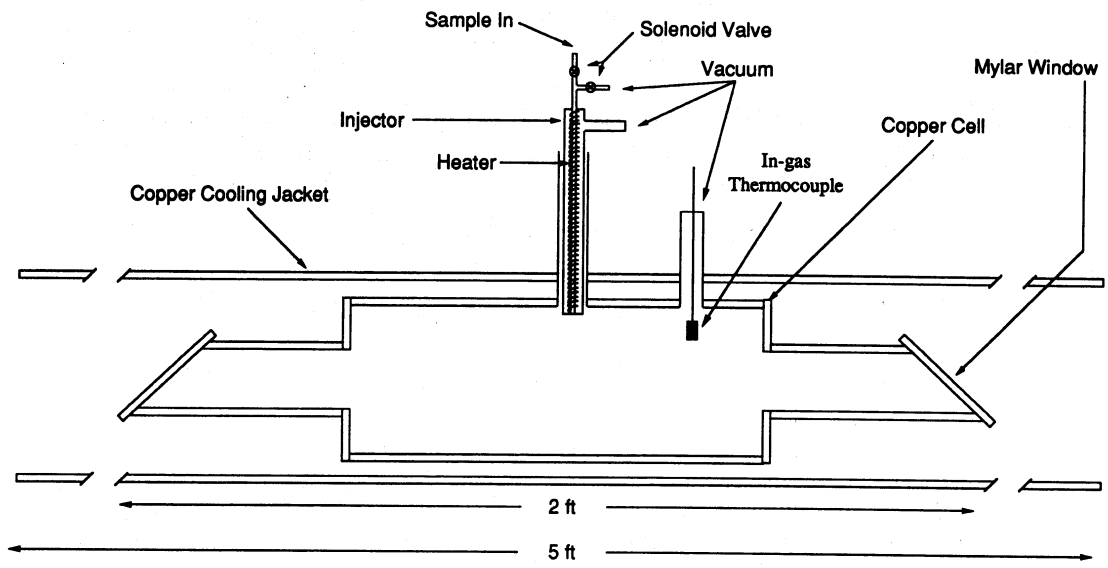

Fig. 1. The collisionally cooled cell and injector assembly used for low temperature experiments.

This cell has been slightly modified from our previous work to provide an in-gas thermocouple for direct gas-temperature measurements. The cell temperature can be varied between 80 and 300 K. The upper temperature limit for data collection is set by the freezing point of the sample gas.

Spectroscopically-active gas, which would have a very low vapor pressure at low temperature, flows into the cell via the injector shown in the center of the cell in Fig. 1. The injector consists of a heated 0.035-in. dia stainless steel tube in a vacuum region separated from the cell by a 0.01-in. thick stainless steel diaphragm. The cell is filled with a static pressure of broadening gas against which the sample gas cools. The sample gas cools rapidly, requiring fewer than 100 collisions to approach the broadening gas temperature, in contrast to the many thousands of collisions required to reach the cell walls where it traps. Pressure of the broadening gas is controlled through a computer controlled valve and was varied between 0.02 and 0.3 torr.

We have previously described the broadband spectrometer and millimeter/submillimeter techniques used in this experiment.[11,12] The output from a computer-controlled 10–15 GHz YIG oscillator is tripled to drive a 1-W, 26–40 GHz TWT amplifier. The output of the TWT is multiplied into the millimeter/submillimeter by a crossed waveguide harmonic generator and propagated quasioptically through the cells described above. The microwaves are then sent into a 1.5 K InSb detector. Pressure measurements are made by an MKS capacitance manometer. Thermal transpiration caused by the temperature difference between the cell and gauge is corrected using the method of Takaishi and Sensui.[13] Pressure corrections in this study were small, typically less than 3%.

The microwave power was swept rapidly in frequency through the absorption line. The bandwidth of the digitizer and detector was large enough to preserve all significant Fourier components. This also preserves the baseline undulations (reflections) which make deconvolution of spectral lineshape difficult. We have therefore used the baseline subtraction technique described in Ref. 9 to reduce this effect in the collisional cooling cell.

For each pressure-broadening parameter, data were recorded at about 30 different pressures. Since the large amount of data would have made a fitting a Voigt profile time consuming, the digitized data were fit to a Lorentzian lineshape with a linear and quadratic term in the baseline. The broadening coefficients were obtained from a least-squares fit to these data with points weighted inversely as the square of the pressure. The measurements were confined to the region where the Doppler contribution was small. The correction for Doppler broadening was subtracted off via the equation,[14]

$$\Delta\nu_o^2 = \Delta\nu_p^2 + \Delta\nu_d^2 \tag{1}$$

Table 1. Measured pressure-broadening parameters.†, ‡, §

$18_{0,18} - 17_{0,17}$			$22_{7,15} - 21_{7,14}$			$29_{0,29} - 28_{0,28}$		
Temperature	$\gamma(O_2)$	$\gamma(N_2)$	Temperature	$\gamma(O_2)$	$\gamma(N_2)$	Temperature	$\gamma(O_2)$	$\gamma(N_2)$
104	6.04	9.11	193	4.46	6.29	113	5.47	7.93
114	5.63	8.41	216	4.25	5.64	130	4.89	7.02
132	5.09	7.80	243	3.87	5.31	193	4.04	5.72
193	4.05	6.12	251	3.51	5.17	216	3.80	5.23
216	4.11	5.88	284	3.24	4.77	243	3.38	5.02
239	3.57	5.58	298	3.25	4.62	251	3.24	4.66
251	3.41	5.18	324	2.96	4.21	284	2.94	4.47
284	3.22	5.10				298	3.19	4.03
298	2.97	4.57				324	2.52	3.72
327	3.03	4.20						
337	2.76	4.76						
354	2.71	4.11						
380	2.28	3.95						

† Temperature in degrees K.

‡ Broadening parameters in MHz/Torr.

§ Absolute uncertainty estimated at ± 10%, relative uncertainty at ± 5%.

where $\Delta\nu_p$ is the pressure broadened line width, $\Delta\nu_o$ is the observed linewidth, and $\Delta\nu_d$ is the Doppler width.

To avoid possible problems with warming of the background gas in the collisional cooling cell, the flow rate of HNO_3 molecules into the cell was kept low. A flow rate analysis, similar to that done in Ref. 9, was done on HNO_3. No observed effects were seen in the measured linewidth with increased flow rate.

RESULTS AND DISCUSSION

Pressure-broadening measurements were made on the $18_{0,18}$–$17_{0,17}$, $22_{7,15}$–$21_{7,14}$, and $29_{0,29}$–$28_{0,28}$ transitions of HNO_3 at the frequencies 231,627.279 MHz, 369,487.272 MHz, and 369,257.890 MHz respectively. Results for broadening by O_2 and N_2 are shown in Table 1. Figures 2, 3 and 4 show the results from Table 1 plotted on linear axis where open squares represent N_2 broadening coefficients and open circles represent O_2 broadening coefficients.

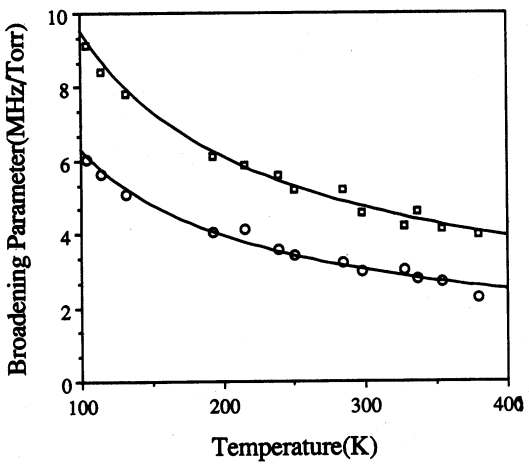

Fig. 2. Measured pressure-broadening parameters of the $18_{0,18}$–$17_{0,17}$ transition of HNO_3 broadened by O_2 (○) and N_2 (□). The solid lines are the result of a least-squares fit to Eq. (2).

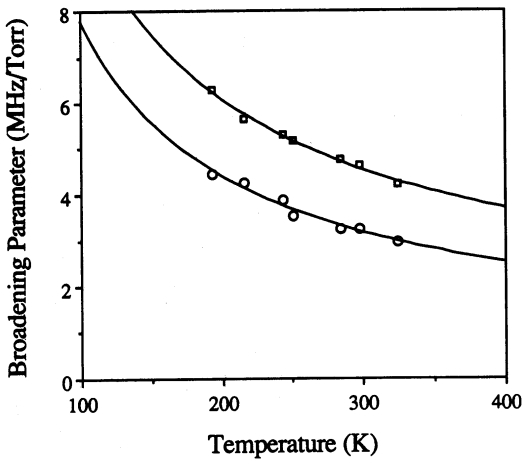

Fig. 3. Measured pressure-broadening parameters of the $22_{7,15}$–$21_{7,14}$ transition of HNO_3 broadened by O_2 (○) and N_2 (□). The solid lines are the result of a least-squares fit to Eq. (2).

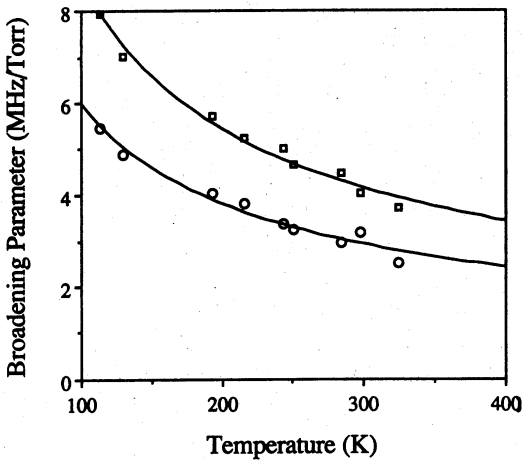

Fig. 4. Measured pressure-broadening parameters of the $29_{0,29}$–$28_{0,28}$ transition of HNO_3 broadened by O_2 (○) and N_2 (□). The solid lines are the result of a least-squares fit to Eq. (2).

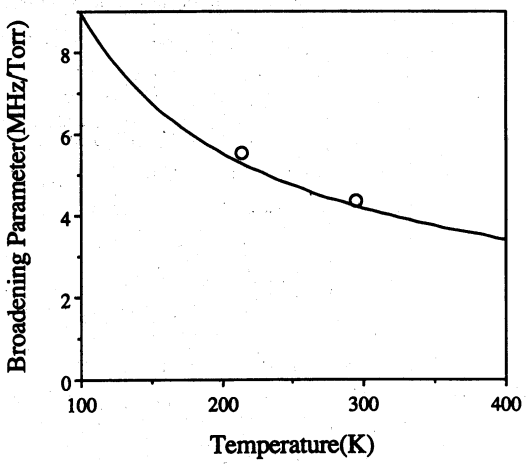

Fig. 5. Average temperature variation of air-broadening parameter. (———) Results of this work; (○) data from Ref. 5.

The data of Table 1 were fit to the power law formula

$$\gamma(T) = \gamma(T_0)[T_0/T]^n, \tag{2}$$

where $\gamma(T_0)$ is the pressure-broadening parameter at reference temperature T_0(300 K) and n is a constant exponent of the temperature ratio. This expression is commonly used to characterize the temperature variation of pressure-broadening parameters.[15] The results for the best-fit parameters are given in Table 2 along with their statistical uncertainties. The results are also plotted as the solid lines in Figs. 2, 3 and 4. The results for temperature coefficients give values from $n = 0.84$ to 0.62. As can be seen from the figures, the previous power law equation adequately describes the variation in the experimental results even down to the lower temperatures.

May and Webster[5] have recently studied the ν_3 and ν_4 vibrational bands of HNO_3 in the i.r. They have made air-broadening measurements at temperatures of 295 and 214 K and have determined a single average pressure-broadening parameter for all of the lines in the vibrational band. Combining our O_2 and N_2 data to obtain air-broadening coefficients and averaging over the three transitions that were studied here, we obtain an average-air broadening parameter of $\gamma(T_0) = 4.16$ MHz/torr (where $T_0 = 300$ K) and $n = 0.70$. The resulting curve is shown in Fig. 5, along with the results from Ref. 5.

As can be seen, there is good agreement between the i.r. data and the microwave results, with the i.r. data falling within 5% of our calculated line. Therefore, the results reported here should be directly applicable in the i.r. and should give a reasonable estimate of the air-broadening parameter of HNO_3 at the temperature and pressure ranges encountered in the upper atmosphere.

Tejwani and Yeung have calculated theoretical air-broadening parameters using Anderson theory.[10] The results of these calculations for the transitions studied here are listed in Table 3 along with the results from this work, where the data from Table 2 and Eq. (2) have been used to calculate

Table 2. Best fit 300 K broadening parameters and n values.†, ‡

	$18_{0,18}$ - $17_{0,17}$		$22_{7,15}$ - $21_{7,14}$		$29_{0,29}$ - $28_{0,28}$	
	O_2	N_2	O_2	N_2	O_2	N_2
γ(300K)	3.01(4)	4.71(7)	3.17(8)	4.51(11)	2.91(7)	4.20(9)
n	0.69(3)	0.64(3)	0.84(10)	0.74(9)	0.67(5)	0.67(4)

† Broadening parameters in MHz/Torr.

‡ Uncertainties are one standard deviation taken from the least squares fit.

Table 3. Air-broadening parameters experiment (this work) vs theory (Ref. 10).†

	$18_{0,18} - 17_{0,17}$		$22_{7,15} - 21_{7,14}$		$29_{0,29} - 28_{0,28}$	
	This work	Ref. 10	This work	Ref. 10	This work	Ref. 10
γ(300K)	4.34	4.60	4.22	4.38	3.91	4.30
γ(200K)	5.64	6.37	5.73	5.72	5.14	5.40

† Broadening parameters in MHz/Torr.

the air-broadening data at 200 and 300 K from the experimental data. As can be seen from the data in Table 3, the variation between theory and experiment range from less than 1% to as large as 13%.

SUMMARY

In this study, we have measured the temperature variation of the pressure-broadening of HNO_3 for the $18_{0,18}$–$17_{0,17}$, $22_{7,15}$–$21_{7,14}$, and $29_{0,29}$–$28_{0,28}$ transitions in the ground vibrational state. Measurements were made for both O_2 and N_2 broadening in the 100–380 K temperature range by the use of a heated equilibrium cell for elevated temperatures and the use of a collisionally cooled cell at the lower temperatures where HNO_3 has a small vapor pressure. The observed pressure-broadening data can be fit to the usual empirical power law, giving n values between 0.62(3) and 0.84(10). Good agreement is seen between the data and previous experimental data obtained in the i.r.

Acknowledgements—We thank W. Ebenstein for his assistance and the Upper Atmosphere Research Program of NASA for support of this work.

REFERENCES

1. R. L. Crownover, R. A. Booker, F. C. DeLucia, and P. Helminger, *JQSRT* **40,** 39 (1988).
2. T. M. Goyette, W. L. Ebenstein, F. C. DeLucia, and P. Helminger, *J. Molec. Spectrosc.* **128,** 108 (1988).
3. C. H. Bair and P. Brockman, *Appl. Opt.* **18,** 4152 (1979).
4. P. Brockman, C. H. Bair, and F. Allario, *J. Appl. Opt.* **17,** 91 (1978).
5. R. D. May and C. R. Webster, *J. Molec. Spectrosc.* **138,** 383 (1989).
6. J. K. Messer and F. C. DeLucia, *Phys. Rev. Lett.* **53,** 2555 (1984).
7. D. R. Willey, R. L. Crownover, D. N. Bittner, and F. C. DeLucia, *J. Chem. Phys.* **89,** 6147 (1988).
8. T. M. Goyette, W. L. Ebenstein, and F. C. DeLucia, *J. Molec. Spectrosc.* **140,** 311 (1990).
9. T. M. Goyette and F. C. DeLucia, *J. Molec. Spectrosc.* **143,** 346 (1990).
10. G. D. T. Tejwani and E. S. Yeung, *J. Chem. Phys.* **68,** 2012 (1978).
11. P. Helminger, J. K. Messer, and F. C. DeLucia, *Appl. Phys. Lett.* **42,** 309 (1983).
12. R. A. Booker, R. A. Crownover, and F. C. DeLucia, *J. Molec. Spectrosc.* **128,** 62 (1988).
13. T. Takaishi and Y. Sensui, *Trans. Faraday Soc.* **59,** 2503 (1963).
14. C. H. Townes and A. L. Schawlow, *Microwave Spectroscopy*, McGraw-Hill, New York, NY (1955).
15. W. S. Benedict and L. D. Kaplan, *J. Chem. Phys.* **30,** 388 (1959).

JOURNAL OF MOLECULAR SPECTROSCOPY 153, 324–339 (1992)

Collisions and Rotational Spectroscopy

THOMAS M. GOYETTE, RODNEY I. MCCORMICK, AND FRANK C. DE LUCIA

Department of Physics, The Ohio State University, Columbus, Ohio 43210

AND

HENRY O. EVERITT III

U.S. Army Research Office, Research Triangle Park, North Carolina 27709

Motivated by Oka's early work on molecular collisions and especially collision-induced rotational transitions, this paper addresses progress in these areas. Particular attention is paid to recent extensions to lower energy collisions of astrophysical significance and to questions about the relation between experimental observables and the more fundamental molecular interactions.

I. INTRODUCTION

The contributions of Professor Takeshi Oka have influenced a number of fields and the careers of many individuals. His pioneering contributions to the field of molecular collisions, and especially their relation to rotational energy transfer, have been of particular interest to us, notably the insights in his article "Collision-Induced Transitions between Rotational Levels," which was published in 1973 (*1*). In this paper we relate this pioneering work to ensuing developments, with particular emphasis on the impact on the physics of lowering the energy of the collisions. More specifically, we seek to address the question, "Is it possible to build a spectroscopic-like interplay between theory and experiment for collisional physics which is analogous to that of rotational spectroscopy?"

II. COLLISIONAL AND RADIATIVE SPECTROSCOPY

At some very fundamental level there is an intimate connection between the familiar radiative spectroscopy and collisional spectroscopy. In the former, molecules are subjected to essentially dipolar radiative fields derived from spectroscopic sources, usually for the purpose of investigating energy level spacings, but also in principle for determining transition rates induced between levels by the interaction between the radiative field and the electric dipole moment of the molecule. In the latter, an electromagnetic field also mediates the interaction, but in a more intimate manner; higher-order multipole moments play a significant role and a continuous spectrum of radiation replaces the essentially monochromatic radiation. This results in a much more complex interplay between the two partners.

In his article Oka emphasized that a means for making progress in the complex field of collisional spectroscopy is to consider limiting cases which simplify the general case. In this regard, perhaps the most important parameters are the strength and time scale of the interaction, considerations which lead to classification of collisions in the

0022-2852/92 $5.00

limits as "hard" (*2*) or "soft" (*3*). More recently, in very low energy collisions, additional phenomena associated with quasibound states have been considered (*4, 5*). The characterization of these collisions requires a more detailed quantum mechanical treatment, but advances in computational power coupled with a reduced number of energetically open collisional channels have made these more complex calculations possible.

It is useful to begin with a consideration of measures of how "classical" or "nonclassical" a process might be. Additionally, since nonclassical effects may be among the most interesting and informative, it is important to seek out the most favorable circumstances for their observation. Clearly, the starting point for such a consideration should be the Correspondence Principle which can be stated as

> The predictions of the quantum theory for the behavior of any physical system must correspond to the prediction of classical physics in the limit in which the quantum numbers specifying the state of the system become very large.

For collisional systems, the appropriate quantum numbers are those specifying the internal states of the molecule and its collision partner and the orbital angular momentum associated with the collisional velocity and impact parameter. An additional consideration is the angular momentum associated with energetically open channels and the averaging over these channels which must take place before any experimentally observable quantity results.

As a numerical example, consider the situation depicted in Fig. 1 in which a helium atom with a kinetic energy corresponding to 300 K and impact parameter 3 Å collides with a CO molecule. For this case a simple calculation shows that $L = 30\ \hbar$. This is a relatively large quantum number and serves as the basic justification for assuming classical paths in semiclassical theories. Similarly, the energy associated with 300 K corresponds to about $J = 10$ for CO, so that the spacing between energy levels is very small in comparison to the thermal quanta and many channels are open energetically.

From this it is easy to conclude that ambient collisions between CO and helium should in many respects be classical and describable by classical or semiclassical theories. An experimental verification of this expectation is provided by the work of Nerf and Sonnenberg, who measured the collision cross section for CO broadened by helium at 294, 195, and 77 K and found them essentially unchanged (*6*). We have found similar results for a wide range of molecules, an example of which is shown in Fig. 2. This constant cross section is the most classical of results, corresponding to a simple billiard ball model.

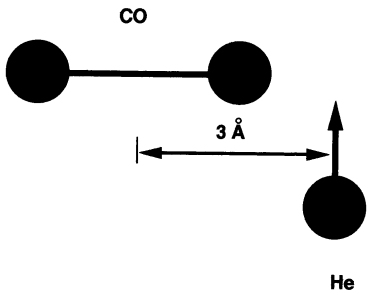

FIG. 1. Helium atom colliding with a CO molecule with an impact parameter of 3 Å.

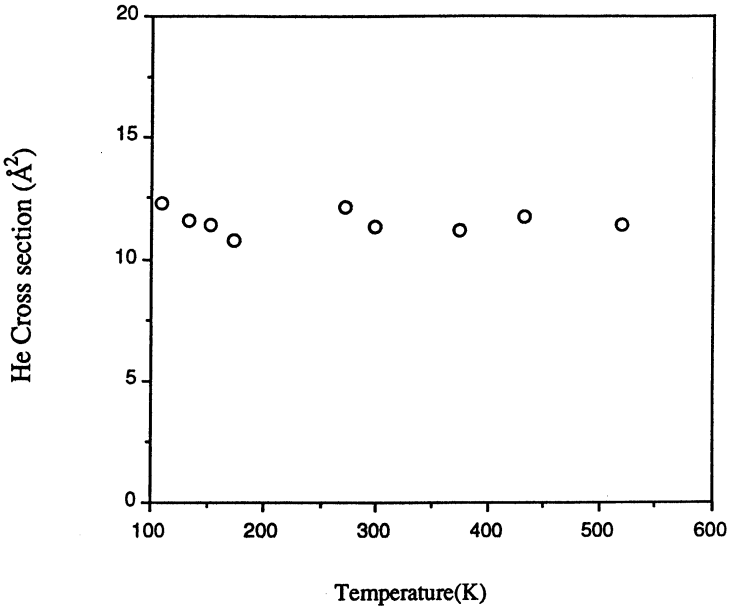

FIG. 2. Helium pressure- broadening cross section as a function of temperature for the $4_{1,4}$–$3_{3,1}$ transition of H_2O.

III. THEORETICAL AND CONCEPTUAL APPROACHES

A useful picture especially applicable to soft collisions can be developed in the context of Anderson theory (*3, 7*). Consider Fig. 3 which shows the collision between an idealized molecule A with two states and transition frequency ω_{ab} and a collision partner B. Here B passes A with velocity v and impact parameter b. The interaction potential can be considered to be of the form

$$V(t) = \frac{K}{r(t)^n}, \tag{1}$$

where $r(t)$ is the time varying distance between A and B, and K and n are constants characteristic of the multipole moment(s) involved. Substituting

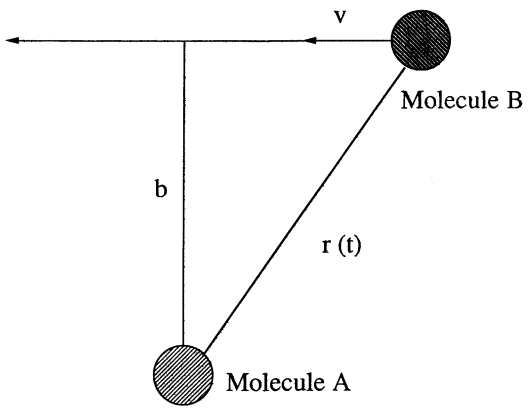

FIG. 3. The basic geometry of a collision in Anderson theory showing the impact parameter b.

$$x \equiv \frac{vt}{b} \qquad k \equiv \frac{b}{v}\omega_{ab} \tag{2}$$

into time-dependent perturbation theory gives the matrix element for the transition probability

$$\langle a|P|b\rangle = \frac{2\pi K}{hb^{n-1}v}\int_{-\infty}^{\infty}\frac{e^{ikx}}{(1+x^2)^{n/2}}\,dx, \tag{3}$$

and for pressure-broadening calculations, the transition probability weighting factor

$$S(b) = |\langle a|P|b\rangle|^2, \tag{4}$$

the pressure-broadening cross section

$$\sigma = \int_0^{\infty} 2\pi b S(b)db, \tag{5}$$

and linewidth

$$\Delta\nu = \frac{Nv\sigma}{2\pi}, \tag{6}$$

where v is the molecular velocity.

Equation (3) is in the form of a Fourier integral and shows the interaction of the multipole moments of the molecule with the spectrum of the collision. For $k \gg 1$, the Fourier components of the radiation produced in the collision do not reach the transition frequencies of A and the contribution to broadening or transition probability is small. In this context it is useful to note that hydrogen and helium have the largest thermal velocities, thereby leading to the smallest k's and the highest-frequency Fourier components. Furthermore, a hard sphere has in effect $n = \infty$ for that class of molecules which come within the sphere's radius R, thereby producing $P = 1$ and the classical collisional cross section

$$\sigma = \int_0^R 2\pi b db = \pi R^2. \tag{7}$$

More exact treatments additionally consider the internal energy levels and multipole moments of the collision partner and orientation effects (*8, 9*).

As an example, consider room temperature collisions between molecules with large electric dipole moments. In this limit the semiclassical theory works well (to within an adjustable scale factor) as shown for the case of Formaldehyde (CH_2O) in Table I (*10*). Inspection of these results shows that the detailed transition to transition variation is reproduced to essentially experimental uncertainty. This semiclassical theory also provides a means of understanding collisions which give rise to variable temperature results more complex than those shown in Fig. 2. Figure 4 shows a typical result for an example in which a small molecule with its own internal degrees of freedom is substituted for helium. Here the cross section initially increases with decreasing temperature, only to fall at the lower temperatures. With the lowering of the temperature of the system, on average the collision partners of the spectroscopic gas are in states for which smaller net energy defects can be realized in the Fourier integral. However, at even lower temperatures the width of the spectrum of the collision narrows so that this gain is overcome by the failure of the spectrum to reach high enough in frequency.

TABLE I

Pressure-Broadening Parameters for Formaldehyde (CH_2O, Also Written H_2CO)[a]

Transition	Observed[b]	Theory
$2_{02} \leftarrow 1_{01}$	22.6(7)	22.6
$2_{12} \leftarrow 1_{11}$	28.9(6)	27.2
$2_{11} \leftarrow 1_{10}$	28.6(6)	27.2
$3_{03} \leftarrow 2_{02}$	20.8 (4)	20.9
$3_{13} \leftarrow 2_{12}$	24.3 (5)	23.6
$3_{12} \leftarrow 2_{11}$	24.5 (6)	23.6
$3_{22} \leftarrow 2_{21}$	30.2 (6)	30.0
$3_{21} \leftarrow 2_{20}$	30.7(8)	30.0
$4_{14} \leftarrow 3_{13}$	23.0(7)	22.7
$4_{13} \leftarrow 3_{12}$	23.1(7)	23.1
$6_{15} \leftarrow 6_{16}$	25.8(11)	25.7
$9_{18} \leftarrow 9_{19}$	28.4(12)	30.0

[a] Data from Ref. 10.
[b] Broadening parameters are in MHz/Torr.

Another factor is important in the comparison between collisional and energy-level spectroscopy. Because the spatial scale of a collision is comparable to the dimensions of the collision partners, the higher-order multipole moments can play a significant role. Conversely, in interactions with external radiation the interaction with the dipole moment is dominant because of the dipole nature of the external field over molecular dimensions.

At lower collision energies new phenomena which are beyond the context of semiclassical models become important. Although several distinguishable cases can be identified, for our purposes they can all be associated with quasibound states. Consider Fig. 5. At high collision energies the molecules effectively bounce off strong repulsive

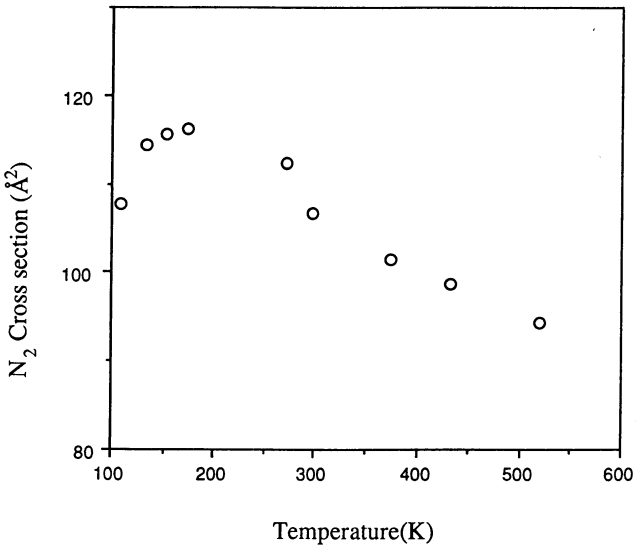

FIG. 4. Cross section for the $4_{1,4}$–$3_{3,1}$ transition of H_2O broadened by N_2 as a function of temperature.

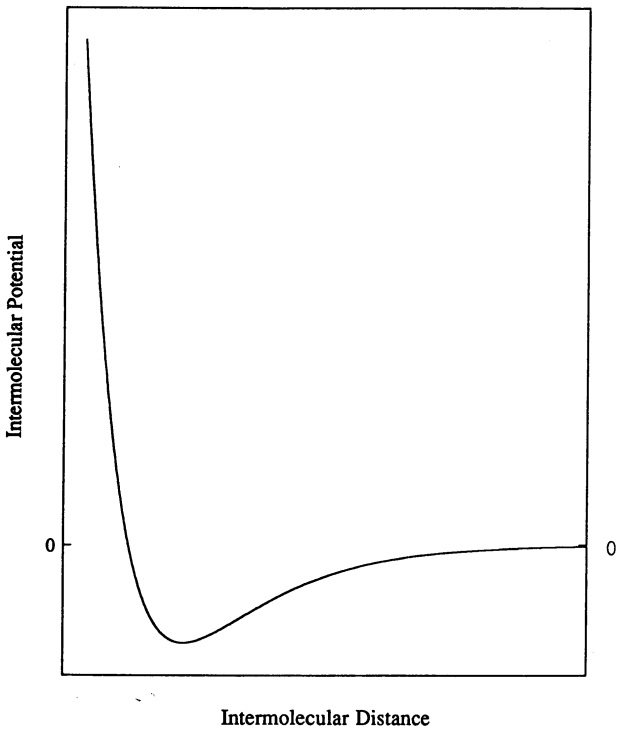

FIG. 5. Slice along one dimension of a typical intermolecular potential.

cores in a fashion represented by the semiclassical theory discussed above. However, at lower energies the existence of the shallow attractive well gives rise to the formation of intermediate states during the collision. In this regime much more exact (and computationally costly) methods are required which quantize the entire problem, including the angular momentum of the molecular trajectories (*4, 5*).

An especially interesting calculation has been done by Palma and Green (*11*) for CO–He collisions and the results are shown in Fig. 6. Using a potential obtained by ab initio techniques, the pressure-broadening cross section was calculated as a function of collision energy. This result is shown as the upper line in this figure. At the lowest energies, large resonances associated with the quasibound states are important. These decrease slowly in size with increasing collision energy, and finally approach the classical plateau associated with higher energy collisions. Palma and Green then reduced the depth of the attractive well by a factor of two and repeated the calculation, producing the results shown by the middle line. The lower line was obtained by completely eliminating the attractive well. These results are extremely useful, providing a basis for substantial qualitative understanding of low energy processes. They show the importance of the shallow attractive well in forming resonances which increase the experimentally observable cross sections. Furthermore, in the case of no well the approach toward zero cross section at zero energy is, at least to the authors, intuitively satisfying.

Figure 7, developed by use of the MOLSCAT computer routines[1] for the CO–He

[1] Private communication from Sheldon Green.

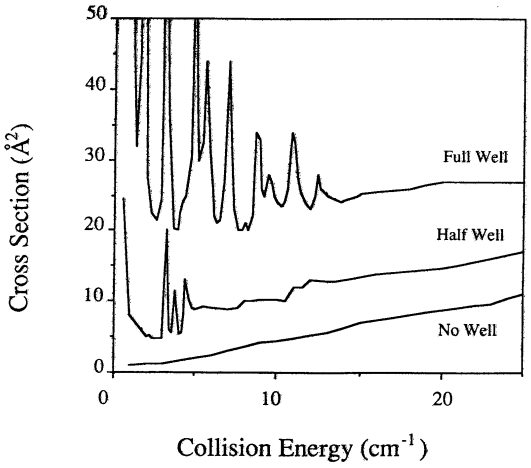

FIG. 6. Pressure-broadening cross sections for the full well, the half well, and no well.

system and using the full well illustrates a number of additional features. In this figure the angular momentum L is the total angular momentum, the good quantum number of the problem. Calculations are done on an L-by-L basis and after each calculation the cross section obtained at that L is added to the sum of all preceding calculations at that energy, thus producing an accumulated cross section as a function of energy and angular momentum. This value is then plotted on the graph of Fig. 7. The most striking observation is that the size of the resonances decreases rapidly with increasing energy, becoming broader and weaker, and eventually approaches a flat plateau beyond the right of the region plotted. Additionally, it can be noted that the resonances saturate with increasing L and that the region of steepest rise (i.e., the region of largest differential cross section) increases gradually in L with increasing energy.

Upon first viewing this, it is easy for those who desire some insight into the physics to be overcome with dismay. However, it is possible to make at least one very simple calculation which restores some of the experimentalist belief that they ought to be able to have some picture of what is being measured. Consider that the angular momentum of the helium in the example above can be given by

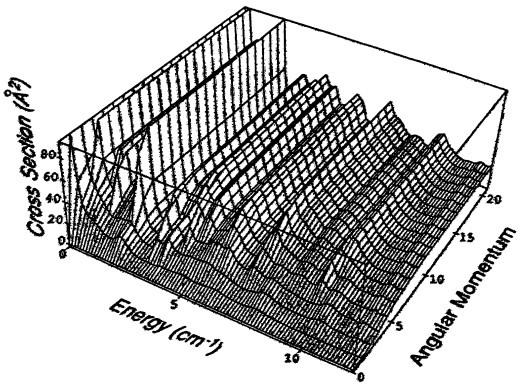

FIG. 7. Plot of the pressure-broadening coefficient for the CO–He system at each energy as a function of the total angular momentum of the calculation.

$$L\hbar = mvb, \tag{8}$$

where L is the quantum number associated with the "orbital" angular momentum, m the mass of the helium atom, v the velocity of the helium atom, and b the impact radius. The kinetic energy E_k of the helium atom is then given by

$$E_k = \tfrac{1}{2}mv^2 \tag{9}$$

and

$$L = \frac{b}{\hbar}\sqrt{2Em}. \tag{10}$$

If Fig. 7 is replotted as a contour plot and the line which is given by Eq. (10) is added, Fig. 8 results. Remarkably, the line lies (with no adjustable parameters) exactly along the maximum in the differential cross sections. Points above the line simply represent cases in which the helium atom misses the CO molecule (too much angular momentum at a given energy results from too great an impact parameter) and points below represent cases where the impact is closer to the center of the molecule (and thus less efficient in the transfer of angular momentum). This is not only a satisfying physical result, but more importantly one which strongly indicates that human intuition about these microscopic processes is still good enough to use as a guide to find interesting paths of scientific inquiry.

IV. AN EXPERIMENTAL APPROACH TO LOW-TEMPERATURE COLLISIONS

In his 1973 article, Oka noted the importance of these very low energy collisions to astrophysical problems, but went on to say that they would probably have to be resolved by theoretical methods because of the difficulty of producing appropriate conditions in the laboratory. However, for the past several years we have made a number of measurements in this regime by use of a technique which we have developed and refer to as collisional cooling. We have discussed this technique in detail elsewhere and only briefly describe it here (*12, 13*). The basic problem lies in the vanishingly small vapor pressures of spectroscopically active gases of primary interest at very low temperatures. This, however, does not preclude their existence in astrophysical contexts. In the laboratory a similar environment, on a very much faster time scale, can be produced by injecting warm, spectroscopically active molecules into a cold background gas (typically helium or hydrogen; or in somewhat higher temperature regimes, nitrogen

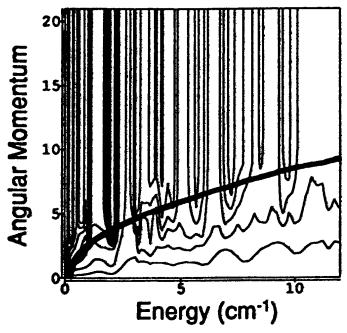

FIG. 8. Contour plot of Fig. 7 with line which is the locus of points of Eq. (10) added.

or oxygen). Elementary calculations show that for spectroscopically useful pressures, the gases cool to the temperature of the background gas very rapidly, and remain in the cell as they diffuse toward the cold walls for a period sufficient to produce concentrations which are easily observable. Although there are other means for producing "cold" gases, this one is particularly attractive because it produces samples of well defined temperature, over macroscopic path lengths, and which are cold in all degrees of freedom (with the possible exception of vibration, an attribute which can be used to advantage in some circumstances) (*14*).

We have now done a number of experiments in this regime, and a summary of results is shown in Fig. 9 (*13, 15–18*). In this figure the observed cross section divided by the cross section at 300 K is plotted in order to show a normalized cross section for which at least a first-order correction for size has been made. The curves shown are each representative of a large number of measurements, all of which are typically within 5% of the plotted lines. These curves are much smoother than the theoretical plots of Figs. 6 and 7 because the experiments are averaged over thermal energy distributions. Although detailed calculations have only been done for two of the cases, CO–He and DCl–He (*18*), it is useful to inquire if the qualitative features of these results can be understood in the context of the ideas and calculations put forth above. As might be expected on the basis of simple theory, those species with the most widely spaced rotational levels do show the smallest normalized cross sections, and for CO, the higher, more widely spaced rotational levels also have smaller cross sections at low temperatures. These observations are clearly consistent with the fact that resonances are related to the number of energetically open channels which form quasibound states. This number should be related to the relative sizes of the molecular energy level spacings and the depth of the attractive well. However, in this context it is somewhat surprising to see how little state to state variation there is in CH_3F given the significantly larger energetic isolation of the higher K lines. Finally, at the lowest temperatures, none of the observed cross sections are increasing with decreasing temperature; many, in fact, show rapidly decreasing cross sections. Although this result

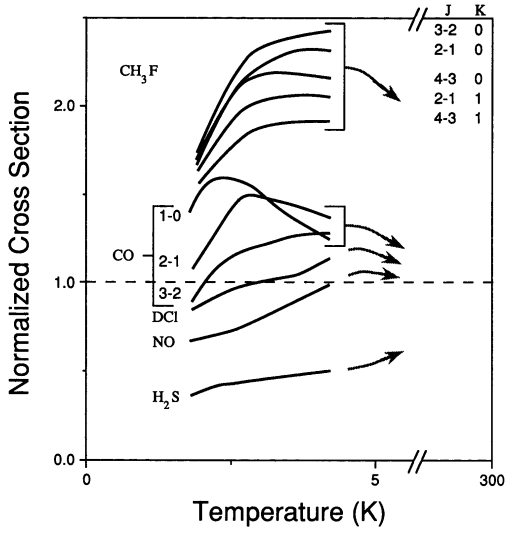

FIG. 9. Observed normalized helium pressure-broadening cross sections for a number of species in the temperature region below 5 K.

is satisfying in the context of the Fourier components of semiclassical theories, the situation in the context of the more exact theories is less clear.

V. STATE-TO-STATE COLLISIONAL TRANSITION RATES

Although pressure broadening and the study of collision-induced rotational transitions are intimately related, Oka clearly recognized that substantially more information can be obtained from the latter. This was a major theme of his 1973 article. Below we discuss a series of experiments which illustrate this point and which are based on the experiment shown in Fig. 10.

The experimental system, which we have previously described (*19–21*), consists of two major subsystems. The spectrometer can probe the absorption profiles of the relevant rotational transitions necessary to map out energy transfer in most molecules. Briefly, it consists of a reflex klystron operating at about 35 GHz, a harmonic generator which produces millimeter/submillimeter radiation at multiples of the klystron fundamental, a diagnostic cell, and an InSb detector. The klystron was phase locked to a frequency synthesizer, and the harmonic generator provided the power at the frequencies required for the diagnostic probe. A high accuracy capacitance manometer was used to determine the amount of gas in the diagnostic cell. The detector has a frequency response of about 1 MHz at its operating temperature of 1.6 K.

The second subsystem was a Q-switched CO_2 laser which produced 500 nsec pulses of 10 μm radiation yielding about 40 W per pulse every 200 μsec. The laser beam entered the diagnostic cell through a ZnSe window and a 3 mm diameter hole. The

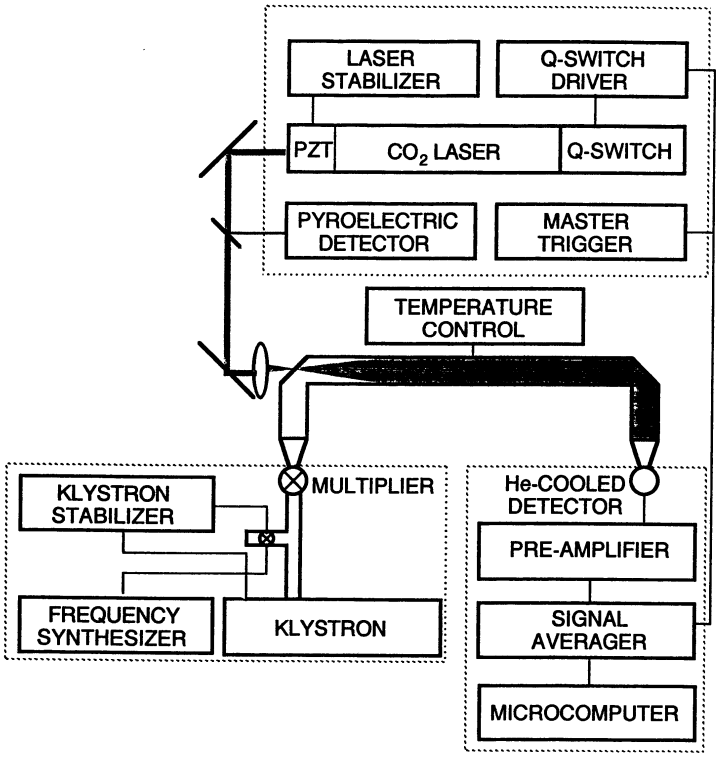

FIG. 10. Block diagram of infrared–millimeter/submillimeter double-resonance experiment.

other end of the cell had a teflon window which acted as a beam dump for the laser radiation while appearing transparent to the mm/submm radiation. The shape of the infrared pulse was monitored by a fast pyroelectric detector, and the average power was measured by an infrared power meter.

The experimental method consists of monitoring the change in strength of a rotational absorption line following pumping of excess population into a rovibrational state of the molecule. To do this the microwave system was locked to the frequency of the rotational transition in question, the laser was pulsed, and the time response of the transition was recorded on a fast digitizer. This time-resolved infrared–millimeter-submillimeter-wave double-resonance technique is extremely powerful for determining state to state energy transfer. The individual rotational transitions studied are easily resolved, the spectrometer is extremely sensitive and highly tunable making many lines accessible, the absorption of a line is easily measured, and the absorption coefficients for rotational transitions are well known. Since the rotational energy levels initially have only small population differences (typically <5%), rotational spectroscopy is extremely sensitive to additional changes in state population. These characteristics make it possible to determine the absolute number densities in essentially all the states of interest in the molecule.

Oka's work describing the propensity of certain interactions predicts that molecular collision dynamics are governed by the symmetry and the dominant multipolar moments of the colliding molecules (*1*). For the symmetric-top molecule CH_3F, the dominant multipolar moment is the dipole moment, which produces the familiar collisional selection rule $\Delta J = 0, \pm 1$, $\Delta K = 0$. Moreover, the C_{3v} symmetry of CH_3F restricts collisions that change the quantum number K by multiples of three. Both of these observations have been experimentally verified in our previous work, and the dipole–dipole interaction was clearly demonstrated to be the dominant multipole–multipole collisional process (*19, 22*). Oka's work also outlined the formalism for calculating the transition matrix elements for higher-order multipole–multipole interactions. In particular, he showed how the maximum quantum change in rotational state is directly related to the order of the interacting multipole moment of the molecule. In our study of collisional transitions with $\Delta J \leqslant 10$, the propensity rules laid out by Oka successfully described the observed processes.

For pairs of molecules with large dipole–dipole interactions, it is clear that these strong interactions so dominate the pressure-broadening process that the deconvolution of higher-order effects is problematic at best. Methyl Fluoride (CH_3F) is an interesting case in point with pressure-broadening parameters similar to those shown in Table I for CH_2O. In this context, we have undertaken a series of time resolved measurements of state to state transition probabilities as a function of temperature and have quantitatively calculated many of the underlying rates. This work has included not only the study of pure rotational processes but also fast vibrational swapping processes which we have found to be important. Collectively, these rates provide a fairly complete map of collision induced rotational energy transfer in this molecule and are shown in Table II (*23*). Inspection shows that there are two dominant rates at room temperature, the rate associated with the electric dipole moment and the rate associated with rotation about the molecular symmetry axis, the $\Delta K = 3n$ rate. The important point is that many other slower rates are quantitatively observable in these state to state measurements. Since many of these rates are more than two orders of magnitude slower than the dominant rates, their contributions to pressure broadening are essentially negligible and would be very difficult to deconvolute from such data.

TABLE II

Collision Induced Transition Rates in CH_3F

	$^{12}CH_3F$	$^{13}CH_3F$
Gas kinetic collision cross section	44[a]	44
Dipole-Dipole cross section at 300K		320 (30)
$\Delta K = 3n$ cross section at 120K	33.1 (16)	46.6 (20)
$\Delta K = 3n$ cross section at 150K	28.6 (78)	47.0 (31)
$\Delta K = 3n$ cross section at 200K	51.1 (57)	54.8 (74)
$\Delta K = 3n$ cross section at 250K	46.0 (42)	74.1 (59)
$\Delta K = 3n$ cross section at 300K		137 (5)
$\Delta K = 3n$ cross section at 350K		190 (40)
$\Delta K = 3n$ cross section at 400K		235 (50)
ν_3 V-swap cross section at 120K	50.6 (10)	54.1 (1)
ν_3 V-swap cross section at 150K	43.4 (20)	52.3 (15)
ν_3 V-swap cross section at 200K	36.4 (21)	36.2 (10)
ν_3 V-swap cross section at 250K	22.8 (9)	30.2 (16)
ν_3 V-swap cross section at 300K	18.9 (15)	21.0 (21)
ν_3 V-swap cross section at 350K	15.6 (10)	16.8 (28)
ν_3 V-swap cross section at 400K	13.4 (35)	13.6 (19)
$\lvert\Delta J\rvert = 2$ weighted cross section at 300K	2.36 (51)	5.10 (45)
$\lvert\Delta J\rvert = 3$ weighted cross section at 300K	1.60 (6)	2.61 (40)
$\lvert\Delta J\rvert = 4$ weighted cross section at 300K	1.14 (7)	1.82 (43)
$\lvert\Delta J\rvert = 5$ weighted cross section at 300K	0.897 (31)	1.27 (20)
$\lvert\Delta J\rvert = 6$ weighted cross section at 300K	0.622 (36)	1.02 (6)
$\lvert\Delta J\rvert = 7$ weighted cross section at 300K	0.510 (20)	
$\lvert\Delta J\rvert = 8$ weighted cross section at 300K	0.489 (25)	
$\lvert\Delta J\rvert = 9$ weighted cross section at 300K	0.438 (20)	
$\lvert\Delta J\rvert = 10$ weighted cross section at 300K	0.418 (15)	
a from SPG law at 300K (Å^2)	0.221 (6)	0.221 (6)
γ from SPG law at 300K	1.22 (3)	1.22 (3)
c for IOS cross sections at 300K (Å^2)	287 (68)	287 (68)
γ for IOS cross sections at 300K	1.30 (5)	1.30 (5)

[a] All cross sections are in Å^2.

While Table II appears to contain a wealth of collisional information, such is not the case. Consider for example the ν_3 vibrational swapping rate (the V-swap) as a function of temperature. All of these rates are derivable from an Anderson-like formulation of Sharma and Brau (*24*) which uses as its input a single dipole moment derivative independently obtainable from other measurements. Figure 11 shows the agreement between the theoretical *prediction* and the observed values from Table II. Only a small adjustment of this parameter is required to reproduce all of these individual rates to within experimental uncertainty.

Similarly, all of the $\Delta J = n$ rates can be calculated from the 'c' and 'γ' constants of the IOS (Infinite Order Sudden) scaling law or the 'a' and 'γ' constants of the SPG (Statistical Power Gap) law (*25*). This leaves, at present, only the $\Delta K = 3n$ processes unexplained on the basis of fundamental parameters. However, since these cross sections are smoothly varying and approach the gas kinetic cross section at the lowest temperatures observed, it seems unlikely that they represent a large amount of independent data about the molecular interaction. Although all of this reduction in the number of parameters required to characterize these temperature-dependent state-to-

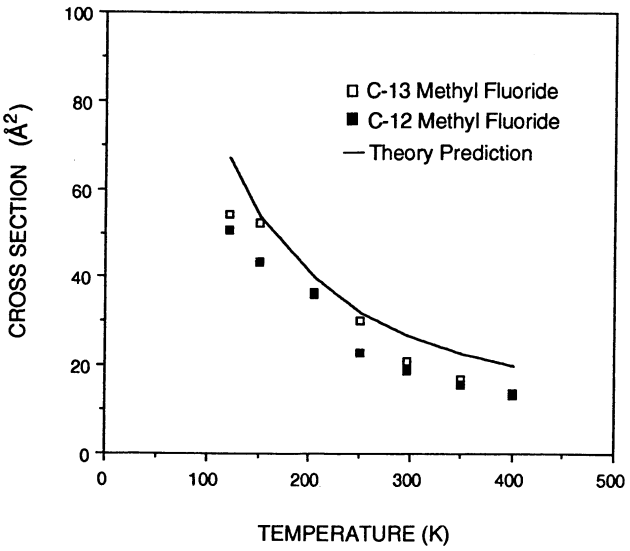

FIG. 11. Comparison between observed vibrational swapping rates for CH_3F and rates calculated via the theory of Ref. (*24*) as a function of temperature.

state processes should be considered to be a significant achievement, it shows that there is not much independent information in the data set which could serve as a basis for a study of the intermolecular potential.

VI. DISCUSSION

It is interesting to raise the question if it is possible to develop spectroscopic-like theories for collisional processes; theories in which a small number of physically well founded constants, defining the intermolecular potential, can be related to a much larger number of observable collisional parameters. In addition, there is both a practical and philosophical question: Is it the goal to use knowledge of the intramolecular potential to predict experimentally observable parameters or to invert the problem and seek fundamental molecular information from measurements of some of these parameters?

The pressure-broadening work on CH_2O discussed above and shown in Table I is in some sense an example of a one constant spectroscopic theory. However, in it the information obtained about the intermolecular potential is limited to the value of the electric dipole moment, a parameter which can be obtained with far greater accuracy via the Stark effect. Next, consider the case of collisions dominated by an electric dipole term in one molecule and an electric quadrupole term in another molecule. An interesting early example is that of the pioneering calculations of Benedict and Kaplan for H_2O broadened by N_2 (*26*). However, values of electric quadrupole moments are much less well known than electric dipole moments, and Benedict and Kaplan used the time-honored spectroscopic technique of fitting the value of the quadrupole moment to the data. However, in this case other higher-order interactions make important contributions, lending uncertainty to both the physical meaning of the fitted quadrupole moment and the accuracy of the prediction for the rest of the cross sections. More recently, we have made a number of measurements of a wide variety of gases with strong electric dipole moments broadened by N_2 and O_2 (*27*).

In cases where there were previous theoretical calculations, significant differences were found, especially for oxygen, which has the smaller quadrupole moment and for which higher-order interactions are presumably more important.

Thus, we conclude that for room-temperature pressure-broadening experiments, semiclassical theories can be spectroscopic when the collisions are dominated by long-range interaction, but in these cases only limited amounts of information are obtained about the intermolecular potential and often that information is available with higher accuracy by other means.

Next, let us consider the more general question of the amount of independent information available. Clearly, in the room-temperature pressure-broadening problems discussed above there is little independent information because, although there is apparently a wide range of experimental data, they can be predicted to experimental accuracy by one or at most a few constants. In many respects this is analogous to energy level spectroscopy in which for heavy asymmetric rotors literally thousands of transitions can be predicted to better than 1% accuracy by three rotational constants. The situation for near-ambient-temperature state-to-state rate measurements is similar, but less clear at this point in time. As discussed above, for the case of CH_3F, a large body of state to state rates can in fact be related to a few fundamental constants. However, at this time the data for the $\Delta K = 3$ processes have not been derived from more fundamental constants and might themselves be fundamental. It is worth noting that at high temperatures the regions of the potential which are sampled by these collisions are simple and perhaps it should not be surprising that these collisions can be described by relatively few parameters. Somewhat more speculatively, it is interesting to note that the $\Delta K = 3n$ process involves rotations about the symmetry axis of CH_3F induced by collisions with the rather complex shape associated with the CH_3 group. Thus, the general question about the amount of information contained in these parameters remains open.

However, as collisional techniques are extended to much lower temperatures the situation with respect to the amount of information becomes qualitatively different. First, the number of independent resolution elements which can be investigated experimentally increases significantly. The spectral "resolution" of a thermal collision is essentially set by the width of the thermal velocity distribution, a fractional quantity. Thus, there is as much spectral space between 2 and 4 K as between 150 and 300 K. Over this very wide range it is meaningful to think in terms of investigating the collisional interaction by tuning the temperature-dependent spectrum of the collision. In addition, over this wide range of energy the collisional process interrogates more of the interaction potential and the information contained therein. Thus we conclude that over the wide energy range from room temperature to a few degrees Kelvin there is potentially more information available about the intermolecular potential. Furthermore, there are more resolution elements to carry this information to experimentally resolvable observables.

We have conducted a series of experiments using MOLSCAT which were designed to address some of these issues. One of the most interesting results is that the size and location of the resonances for CO–He collisions are extremely sensitive to details of the potential; locations of spectral lines are much less dependent on the values of rotational constants. In fact, even if given an ideal, nonthermally averaged collision spectrum it is not clear that one could devise a means of adjusting the intermolecular potential to converge to the correct answer. Although it is tempting to deduce that

the wealth of spectral information shown in Figs. 6 and 7 imply a wealth of information about the more basic interaction potential, there is no evidence that this is the case.

More recently, very interesting and enlightening close-coupled calculations have been done for HDO–He (*28*). HDO is a species with much wider rotational energy level spacing than CO and provides an additional test of some of the ideas discussed above. These calculated cross sections show a slow continuous decline below 300 K until energies which correspond to about 10 K are reached. Here resonances appear which significantly raise the values of the cross section. Because there are so few of these resonances, they survive the thermal averaging and produce significant structure in the thermally averaged pressure-broadening cross sections.

A straightforward conclusion that follows from comparing the CO–He and HDO–He cases is that the former has a more complex spectrum, not because of an inherently more complex interaction potential, but rather because its more closely spaced rotational levels lead to more energetically open channels and more resonances. Thus, it would appear that if the goal is to use the spectrum of the collision to learn about the intermolecular potentials via observation of the resonances an appropriate density of rotational states is also needed. If the states are too closely spaced relative to the depth of the attractive well, an exceedingly dense, complex, and sensitive spectrum results; one that is perhaps unassignable. On the other hand, if the levels are too widely spaced, it is possible that no resonances will be observable and this source of information about the intermolecular potential will remain untapped.

Finally, let us consider how many parameters are required to characterize the intermolecular potential. There is the analogous question in energy level spectroscopy. In both cases the answer clearly depends on the range of validity as well as the accuracy required for the task at hand. To take an example from energy level spectroscopy once again, diatomic molecules can be characterized by Morse potentials or Dunham potentials. In the former case, a small number of constants provides a reasonably good model over a very wide range of internuclear distances. In the latter, arbitrary accuracy is obtainable, but at the expense of a much larger constant set and a very reduced range of applicability. Similarly, numerical surfaces produced by fitting large expansions in Legendre polynomials to the results of ab initio calculations of the intermolecular potentials are often used as starting points for detailed collision calculations. However, much simpler potentials based on more analytical approaches have also been used (*5*). Although there is no question that the potentials produced by ab initio calculations are superior, it is not as clear that the number of parameters in them are representative of the amount of independent information.

Thus, in the end we suggest that the answer to the question, "Is it possible to build a spectroscopic-like interplay between theory and experiment for collisional physics?" is clearly yes. However, just as in energy level spectroscopy the answer is only meaningful in the context of a specification of the accuracy and range of validity required.

ACKNOWLEDGMENTS

We thank the Army Research Office and the National Science Foundation for their support of this work.

RECEIVED: January 24, 1992

REFERENCES

1. T. OKA, *in* "Advances in Atomic and Molecular Physics" (D. R. Bates and I. Estermann, Eds.), Vol. 9, Academic Press, New York, 1973.

2. J. H. VAN VLECK AND V. F. WEISSKOPF, *Rev. Mod. Phys.* **17,** 227–236 (1945).
3. P. W. ANDERSON, *Phys. Rev.* **76,** 647–661 (1949).
4. A. M. ARTHURS AND A. DALGARNO, *Proc. R. Soc. London* **256,** 540–551 (1960).
5. S. GREEN AND P. THADDEUS, *Astrophys. J.* **205,** 766–785 (1976).
6. R. B. NERF AND M. A. SONNENBERG, *J. Mol. Spectrosc.* **58,** 474–478 (1975).
7. C. H. TOWNES AND A. L. SCHAWLOW, "Microwave Spectroscopy," McGraw-Hill, New York, 1955.
8. R. R. GAMACHE AND L. S. ROTHMAN, *J. Mol. Spectrosc.* **128,** 360–369 (1988).
9. C. J. TSAO AND CURNUTTE, *J. Quant. Spectrosc. Radiat. Transfer* **2,** 41–91 (1962).
10. R. B. NERF, JR., *J. Mol. Spectrosc.* **58,** 451–473 (1975).
11. A. PALMA AND S. GREEN, *J. Chem. Phys.* **85,** 1333–1335 (1986).
12. J. K. MESSER AND F. C. DE LUCIA, *Phys. Rev. Lett.* **53,** 2555–2558 (1984).
13. D. R. WILEY, R. L. CROWNOVER, D. N. BITTNER, AND F. C. DE LUCIA, *J. Mol. Spectrosc.* **133,** 182–192 (1989).
14. T. M. GOYETTE, W. L. EBENSTEIN, AND F. C. DE LUCIA, *J. Mol. Spectrosc.* **140,** 311–321 (1990).
15. D. R. WILLEY, T. M. GOYETTE, W. L. EBENSTEIN, D. N. BITTNER, AND F. C. DE LUCIA, *J. Chem. Phys.* **91,** 122–125 (1989).
16. D. R. WILEY, R. L. CROWNOVER, D. N. BITTNER, AND F. C. DE LUCIA, *J. Chem. Phys.* **89,** 1923–1928 (1988).
17. D. R. WILEY, R. L. CROWNOVER, D. N. BITTNER, AND F. C. DE LUCIA, *J. Chem. Phys.* **89,** 6147–6149 (1988).
18. D. R. WILLEY, V-E. CHOONG, AND F. C. DE LUCIA, *J. Chem. Phys.*, in press.
19. R. I. MCCORMICK, F. C. DE LUCIA, AND D. D. SKATRUD, *IEEE J. Quantum Electron.* **QE-23,** 2060–2068 (1987).
20. W. C. KING AND W. GORDY, *Phys. Rev.* **90,** 319–320 (1953).
21. P. HELMINGER, J. K. MESSER, AND F. C. DE LUCIA, *Appl. Phys. Lett.* **42,** 309–310 (1983).
22. H. O. EVERITT AND F. C. DE LUCIA, *J. Chem. Phys.* **92,** 6480–6491 (1990).
23. H. O. EVERITT, III, Ph.D. Dissertation, unpublished, Duke University, 1990.
24. R. D. SHARMA AND C. A. BRAU, *J. Chem. Phys.* **50,** 924–930 (1969).
25. N. SMITH AND D. E. PRICHARD, *J. Chem. Phys.* **74,** 3939–3946 (1981).
26. W. S. BENEDICT AND L. D. KAPLAN, *J. Chem. Phys.* **30,** 388–399 (1959).
27. T. M. GOYETTE, W. L. EBENSTEIN, F. C. DE LUCIA, AND P. HELMINGER, *J. Quant. Spectrosc. Radiat. Transfer.* **40,** 129–134 (1988).
28. S. GREEN, private communication.